Int J Thermophys (2007) 28:2128–2144
DOI 10.1007/s10765-007-0285-9

Radiative Properties of Blackbody Calibration Sources: Recent Advances in Computer Modeling

Alexander V. Prokhorov · Sergey N. Mekhontsev · Leonard M. Hanssen

Published online: 16 October 2007

Abstract The radiative characteristics (spectral effective emissivity, spectral radiance, and radiance temperature) of blackbody calibration sources widely used in radiation thermometry are an important subject for advanced computer modeling by the Monte Carlo method. An algorithm and code for stochastic modeling of the radiant heat transfer inside cavities has been developed on the basis of the reciprocity principle and backward ray tracing. The importance sampling technique has been applied to generate the reflected rays according to the surface reflection model that can be a linear combination of the following primary models: Lambertian, Specular, and TETRA (a microfacet model of random tetrahedral pits that mimics reflections from a rough surface). A wide range of axisymmetrical cavities, cylindrical cavities with an inclined flat bottom, and a rectilinear grooved radiator of polygonal profile have been implemented. Various conditions of observation can be modeled to compute appropriate radiation characteristics. A number of different temperature distributions can be assigned to the same node set on the cavity surface, so several related tasks can be modeled in a single run. The results obtained for the radiative properties of isothermal and non-isothermal non-diffuse blackbodies used for the calibration of infrared radiation thermometers are presented and discussed.

Keywords Blackbody · Emissivity · Monte Carlo method · Ray tracing

A. V. Prokhorov · S. N. Mekhontsev · L. M. Hanssen (✉)
Optical Technology Division, National Institute of Standards and Technology, 100 Bureau Dr., Build. 220/A305, MS 8442, Gaithersburg, MD 20899, USA
e-mail: hanssen@nist.gov

A. V. Prokhorov
Joint NIST/USURF Program in Optical Sensor Calibration, Utah State University Research Foundation, North Logan, UT 84341, USA

1 Introduction

Blackbody sources of nearly Planckian radiation (imperfect blackbodies) are often used for calibration purposes in radiation thermometry, optical radiometry, heat flux measurements, and related areas. Typically, such a source is an almost isothermal cavity with a small opening; the characteristics of the output thermal radiation approach those of a perfect blackbody due to multiple reflections of radiation inside the cavity. The spectral radiative characteristics of a cavity can be computed with the help of Planck's law; the appropriate correction factor is the spectral effective emissivity. The directional spectral effective emissivity is defined by the equation,

$$\varepsilon_{\mathrm{e}}(\lambda, T, \boldsymbol{\xi}, \boldsymbol{\omega}) = \frac{L_{\lambda}(\lambda, \boldsymbol{\xi}, \boldsymbol{\omega})}{L_{\lambda,\mathrm{bb}}(\lambda, T)}, \tag{1}$$

where L_{λ} and $L_{\lambda,\mathrm{bb}}$ are the spectral radiance (in $\mathrm{W}\cdot\mathrm{m}^{-3}\cdot\mathrm{sr}^{-1}$) for a wavelength λ of a cavity (possibly non-isothermal) and a perfect blackbody at temperature T, ξ is the point on the cavity radiating surface, and ω is the direction of observation.

The directional spectral effective emissivity is the primary cavity radiation characteristic; the other types of effective emissivities can be computed by averaging over the spectral, spatial, and/or angular domains. Generally, the effective emissivity depends on the cavity geometry, the optical properties of the cavity walls, the temperature distribution over the radiating surface, and the conditions of observation.

Another important quantity is the radiance temperature T_{S} that is defined as the perfect blackbody temperature, for which the spectral radiance at the specified wavelength λ has the same value as for the thermal radiator considered. For an imperfect blackbody having the spectral effective emissivity ε_{e}, the radiance temperature can be computed as

$$T_{\mathrm{S}}(\lambda, T, \boldsymbol{\xi}, \boldsymbol{\omega}) = c_2 \left\{ \lambda \ln \left[1 + \frac{\exp\left(\frac{c_2}{\lambda T}\right) - 1}{\varepsilon_{\mathrm{e}}(\lambda, T, \boldsymbol{\xi}, \boldsymbol{\omega})} \right] \right\}^{-1}, \tag{2}$$

where $c_2 = 1.438769 \times 10^{-2}\,\mathrm{m}\cdot\mathrm{K}$ is the 2nd radiation constant.

For a cavity with specular walls, the effective emissivity can be calculated using an inverse ray tracing procedure, where rays start at the observation point and undergo multiple reflections from the cavity walls. If the cavity walls are perfectly diffuse (Lambertian), the effective emissivity can be found by solving the Fredholm integral equations of the second kind. These methods were reviewed in detail by Bedford in 1988 [1]. However, the reflection from real-world surfaces is neither perfectly diffuse nor perfectly specular, and these approximations are not always sufficient to compute the effective emissivity with uncertainties less than several hundredths of a percent, as required by modern radiometric and pyrometric applications.

In recent decades, the Monte Carlo method has become the most frequently used tool for effective emissivity modeling [2]. Although the stochastic modeling of an arbitrary angular distribution of reflected radiation is possible in principle, the simplest uniform specular–diffuse model has been employed in most published studies [3–7].

This is explained not only by the lack of reliable measurements of optical properties but also by difficulties encountered in the development of modeling algorithms.

Toor and Viskanta [8] modeled the reflection from rough surfaces using Beckmann [9] theory that gives exact results only for single scattering, i.e., for small incident angles and sufficiently smooth surfaces. Unfortunately, details of the modeling algorithm were omitted. Almost 30 years later, Tomitani [10] used a similar approach in combination with the acceptance–rejection method.

Zaworski et al. [11] measured and computed the spatial distribution of radiation passing through a rectangular gap with a rough wall. The polar and azimuthal spherical coordinates for the specular lobe were considered as Gaussian variates counting from the specular direction and with the standard deviations fitted to experimental data. A significant discrepancy between the modeled and measured distributions was obtained. The authors explained this discrepancy as due to a lack of measured values of bi-directional reflectance at large incident angles and the imperfection of the model adopted.

Zhou et al. [12] applied the modified Ward's model of reflection [13] to Monte Carlo modeling of the effective emissivity of a silicon wafer. The model employed requires further improvement because it shows a dependence of directional-hemispherical reflectance (DHR) on incident angle that contradicts experimental data.

Prokhorov and Hanssen [14] described an algorithm based on microfacet theory to model the reflection from rough surfaces. The central idea is to randomly perturb the normal vector to the surface for each incident ray, and to compute the direction of the specular reflection using this perturbed normal. Multiple reflections are replaced by a Lambertian component to maintain energy conservation. The proposed model exhibits experimentally observed effects such as off-specular peaks and increased reflectance near grazing incidence. Adherence to the reciprocity principle for moderate roughness is demonstrated via comparison of forward and backward ray-tracing results (residual discrepancy of several percent).

This article has two main objectives: (i) to describe the state-of-the-art algorithm and code developed at the National Institute of Standards and Technology for stochastic modeling of the radiant heat transfer inside cavities and (ii) to demonstrate, by example, that one should take into account the real angular distributions of emitted and reflected radiation to insure accurate and reliable calculations of the radiative characteristics of blackbody calibration sources.

2 Stochastic Models for Radiation Properties

2.1 Basic Definitions

The radiative properties of a surface are completely described by the spectral bi-directional reflectance distribution function (BRDF) [15] that can be defined in two equivalent forms:

$$f\left(\lambda, \theta_{\mathrm{i}}, \varphi_{\mathrm{i}}, \theta_{\mathrm{r}}, \varphi_{\mathrm{r}}\right) = \frac{\mathrm{d}L_{\lambda,\mathrm{r}}\left(\lambda, \theta_{\mathrm{r}}, \varphi_{\mathrm{r}}\right)}{\mathrm{d}E_{\lambda,\mathrm{i}}\left(\lambda, \theta_{\mathrm{i}}, \varphi_{\mathrm{i}}\right)} = \frac{\mathrm{d}L_{\lambda,\mathrm{r}}\left(\lambda, \theta_{\mathrm{r}}, \varphi_{\mathrm{r}}\right)}{\mathrm{d}L_{\lambda,\mathrm{i}}\left(\lambda, \theta_{\mathrm{i}}, \varphi_{\mathrm{i}}\right)\cos\theta_{\mathrm{r}}}, \tag{3}$$

where λ is the wavelength, $L_{\lambda,\mathrm{i}}$ is the spectral radiance of the incident beam, $L_{\lambda,\mathrm{r}}$ is the spectral radiance of the reflected radiation, $E_{\lambda,\mathrm{i}}$ is the spectral irradiance (in $\mathrm{W}\cdot\mathrm{m}^{-3}$) from the incident radiation, and $(\theta_\mathrm{i}, \varphi_\mathrm{i})$ and $(\theta_\mathrm{r}, \varphi_\mathrm{r})$ are the directions of incidence and observation, respectively, defined by their spherical coordinates.

The BRDF must obey the energy conservation law:

$$\rho\left(\lambda, \theta_\mathrm{i}, \varphi_i\right) = \int_{\varphi_\mathrm{r}=0}^{2\pi} \int_{\theta_\mathrm{r}=0}^{\pi/2} f\left(\lambda, \theta_\mathrm{i}, \varphi_\mathrm{i}, \theta_\mathrm{r}, \varphi_\mathrm{r}\right) \sin\theta_\mathrm{r} \cos\theta_\mathrm{r} \mathrm{d}\theta_\mathrm{r} \mathrm{d}\varphi_\mathrm{r} \leq 1, \tag{4}$$

where $\rho\left(\lambda, \theta_\mathrm{i}, \varphi_\mathrm{i}\right)$ is the spectral DHR; and the spectral directional emissivity of an opaque body is equal to

$$\varepsilon\left(\lambda, \theta_\mathrm{i}, \varphi_\mathrm{i}\right) = 1 - \rho\left(\lambda, \theta_\mathrm{i}, \varphi_\mathrm{i}\right). \tag{5}$$

The BRDF should be consistent with the reciprocity principle;

$$f\left(\lambda, \theta_\mathrm{i}, \varphi_\mathrm{i}, \theta_\mathrm{r}, \varphi_\mathrm{r}\right) = f\left(\lambda, \theta_\mathrm{r}, \varphi_\mathrm{r}, \theta_\mathrm{i}, \varphi_\mathrm{i}\right). \tag{6}$$

If the angular distribution of the emitted or reflected radiant intensity is known, it is possible to construct a simplest stochastic model by generating random rays uniformly distributed in a hemisphere and by assigning to each ray a statistical weight equal to the value of the radiant intensity distribution for this direction. However, such a model is extremely inefficient from the computational point of view, especially for distributions with significant non-uniformities. For effective modeling, the stochastic model of BRDF that is incorporated into a Monte Carlo ray tracing algorithm should provide importance sampling [16], i.e., generating random directions $(\theta_\mathrm{r}, \varphi_\mathrm{r})$ of reflection from a general population having a probability density function equal to $f\left(\theta_\mathrm{i}, \varphi_\mathrm{i}, \theta_\mathrm{r}, \varphi_\mathrm{r}\right) \cos\theta_\mathrm{r}$.

2.2 Specular BRDF

Specular reflection simulates the reflection from a planar, perfectly smooth, mirror-like surface. This is a deterministic process that requires no random variate modeling. If $\boldsymbol{\omega}_\mathrm{i}$ and $\boldsymbol{\omega}_\mathrm{r}$ are unit vectors of incident and reflection directions, respectively, and $\mathbf{n}$ is the normal to the surface, then

$$\boldsymbol{\omega}_\mathrm{r} = \boldsymbol{\omega}_\mathrm{i} - 2\mathbf{n}\left(\boldsymbol{\omega}_\mathrm{i} \cdot \mathbf{n}\right). \tag{7}$$

The BRDF of the specular reflection is expressed by the equation,

$$f_\mathrm{S}\left(\lambda, \theta_\mathrm{i}, \varphi_\mathrm{i}, \theta_\mathrm{r}, \varphi_\mathrm{r}\right) = \rho\left(\lambda, \theta_\mathrm{i}\right) \frac{\delta\left(\theta_\mathrm{r} - \theta_\mathrm{i}\right) \delta\left(\varphi_\mathrm{r} - \varphi_\mathrm{i} \pm \pi\right)}{\sin\theta_\mathrm{r} \cos\theta_\mathrm{i}}, \tag{8}$$

where δ is Dirac's delta-function; $\rho\,(\lambda, \theta_{\rm i})$ is the spectral DHR that might be found by the interpolation of experimental data obtained for a discrete set of incident angles, or computed using Fresnel's law and optical constants n_λ and k_λ.

2.3 Lambertian BRDF

The BRDF for perfectly diffuse (Lambertian) reflection is described by the equation,

$$f_{\rm L}\,(\lambda, \theta_{\rm i}, \varphi_{\rm i}, \theta_{\rm r}, \varphi_{\rm r}) = \frac{\rho\,(\lambda)}{\pi}, \tag{9}$$

where $\rho(\lambda)$ is the spectral hemispherical reflectance that does not depend on incident angle.

Cartesian coordinates of a random vector $\boldsymbol{\omega}_{\rm r}$ can be obtained with the help of the following procedure. A pseudo-random number generator gives a pair of numbers u_x and u_y, uniformly distributed on the segment (0, 1]. Then, they are transformed to two coordinates of the reflected ray in the Cartesian coordinate system:

$$\omega_{{\rm r}x} = 2u_x - 1, \tag{10}$$

$$\omega_{{\rm r}y} = 2u_y - 1. \tag{11}$$

This pair is accepted if $\omega_{{\rm r}x}^2 + \omega_{{\rm r}y}^2 < 1$ and rejected otherwise (in which case, the procedure is repeated). The third component of $\boldsymbol{\omega}_{\rm r}$ can be found from

$$\omega_{{\rm r}z} = +\sqrt{1 - \omega_{{\rm r}x}^2 - \omega_{{\rm r}y}^2}. \tag{12}$$

Another, slightly slower method to generate the random direction of a diffusely reflected ray in the local spherical coordinate system is described in the literature (for instance, see monograph [17]).

2.4 TETRA BRDF Model

The model, which we have named TETRA, is based on ray optics and a micro-facet model of reflections from isotropic randomly rough surfaces. The TETRA BRDF is modeled by specular reflections from random tetrahedron pits generated "on the fly" for each incident ray. In a determinate sense, this model is a three-dimensional (3D) analog of the well-known Torrance–Sparrow model [18] that provides an analytical expression for in-plane angular distributions of radiation reflected by an isotropic randomly rough surface. We assume that the triangular base of each tetrahedron lies in the tangent plane to the surface at the point of ray incidence (see Fig. 1). We also assume that the base triangle sides have random lengths l_1, l_2, and l_3 with a Gaussian probability density,

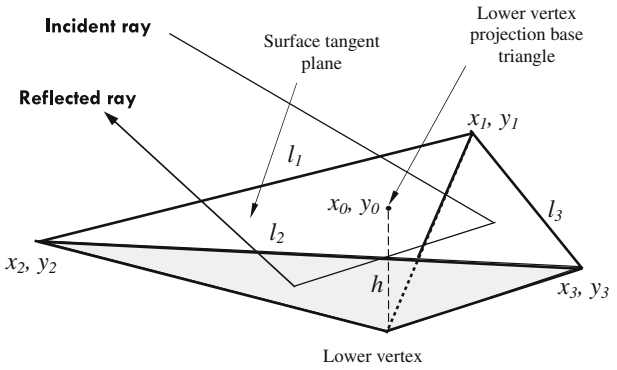

Fig. 1 Tetrahedral pit with a triangular base in the surface tangent plane

$$p(l) = \frac{1}{\sigma_l \sqrt{2\pi}} \exp\left(-\frac{(l-\mu_l)^2}{2\sigma_l^2}\right), \tag{13}$$

where $\mu_l = 1$ is the mean value (can be considered as a measure) and σ_l is the standard deviation.

The triad of random line segments is accepted if their lengths satisfy the following inequalities and rejected otherwise (the "triangle rule"):

$$l_1 + l_2 > l_3 \quad \text{and} \quad l_2 + l_3 > l_1 \quad \text{and} \quad l_3 + l_1 > l_2. \tag{14}$$

Numerical experiments show the dependence of the BRDF shape on σ_l. However, the time of computation grows significantly when $\sigma_l >> 1$. For our discussion, we select $\sigma_l = 1$.

We studied several variants for arranging the point (x_0, y_0) for projection of the lower tetrahedron's vertex onto the base plane (see Fig. 2): R—a random point uniformly distributed inside the triangle; G—the base triangle centroid (center of gravity); V—one of the vertices of the base triangle; C—the circumcircle center, as well as several others left out of the scope of this article. We found that each variant yields its own unique family of BRDF curves and increases the overall flexibility of the TETRA model to simulate scattering from a variety of material types.

After determining the point(x_0, y_0), the random depth h of the tetrahedral pit and $z_0 = -h$ are found. We used the two-parameter Weibull-probability density defined as

$$p(h) = \frac{\beta}{\eta^\beta} h^{\beta-1} \exp\left[-\left(\frac{h}{\eta}\right)^\beta\right], \quad h > 0, \tag{15}$$

where $\beta > 0$ is the shape parameter and $\eta > 0$ is the scale parameter of the distribution. We also call η *the roughness parameter* because the following relationship is known [19]:

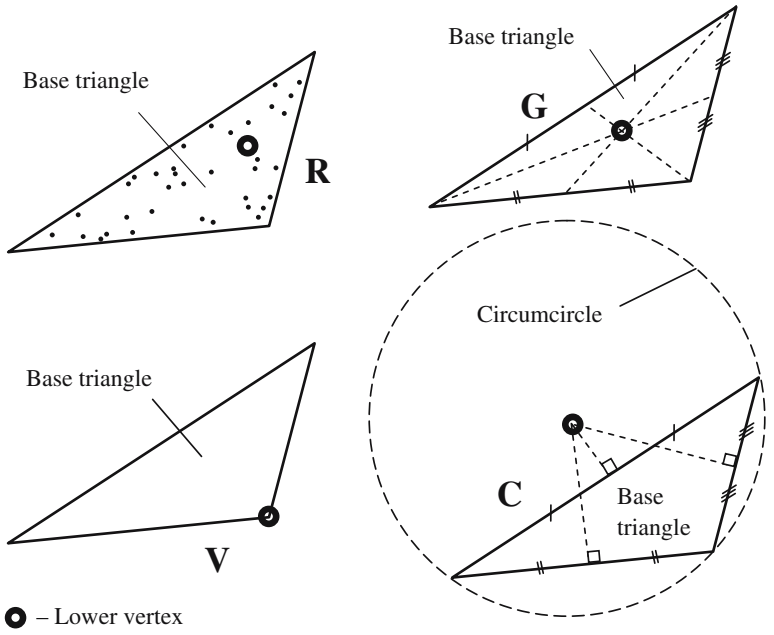

Fig. 2 Various types of arrangement for the projection of the lower tetrahedron's vertex onto the plane of the base triangle: (R—a random point uniformly distributed inside triangle; G—the base triangle centroid (center of gravity); V—one of vertices of base triangle; C—the circumcircle center)

$$\sigma^2 = \eta^2 \left\{ \Gamma\left(1 + \frac{2}{\beta}\right) - \left[\Gamma\left(1 + \frac{1}{\beta}\right)\right]^2 \right\}, \tag{16}$$

where σ is the rms roughness (standard deviation of the Weibull distribution); $\Gamma(x)$ is the gamma function of the real argument x.

If $\beta = 1$, we have the exponential distribution; for $\beta = 2$, the Weibull distribution becomes the Rayleigh distribution. The values of β from the interval $1 \leq \beta \leq 2$ produce the physically plausible BRDF shapes. To generate the Weibull-distributed random variate w, a random variate u drawn from the uniform distribution in the interval (0, 1] must be transformed [20] to

$$w = \eta \left(-\ln u\right)^{1/\beta}. \tag{17}$$

We selected the point of intersection of the incident ray with the base plane as a random point uniformly distributed inside the base triangle using the algorithm from Ref. [21]. To ensure the random orientation of the base triangle and isotropy of the modeled surface, the tetrahedron was rotated through a random angle around a vertical axis passing through the point of intersection of the incident ray and the base plane.

The incident ray undergoes multiple reflections from the internal facets of the tetrahedron, and after each reflection, the radiance of the ray is multiplied by the DHR of the facet. The algorithm [22] was employed to test whether the intersection of the ray with

the plane is inside the facet triangle. This random process continues until the ray leaves the tetrahedral pit, or the radiance becomes less than the prescribed threshold value.

We investigated the TETRA BRDF behavior using a "virtual goniophotometer" [23,24]: a computer program that enables us to compute the mean radiance of the radiation reflected by a surface into the small solid angle associated with the direction (θ_r, φ_r) and to perform a numerical integration over the complete hemisphere to obtain the value of DHR. The second method for computation of the DHR is an energy summation of all rays reflected by the tetrahedral pit to the upper hemisphere. The coincidence of the DHR computed by the two methods is additional evidence of the accuracy of the calculations. Typical 2D plots (in-plane section) for four variants of the TETRA BRDFs generated for $\beta = 2$, $\eta = 0.1$ and three incident angles are shown in Fig. 3.

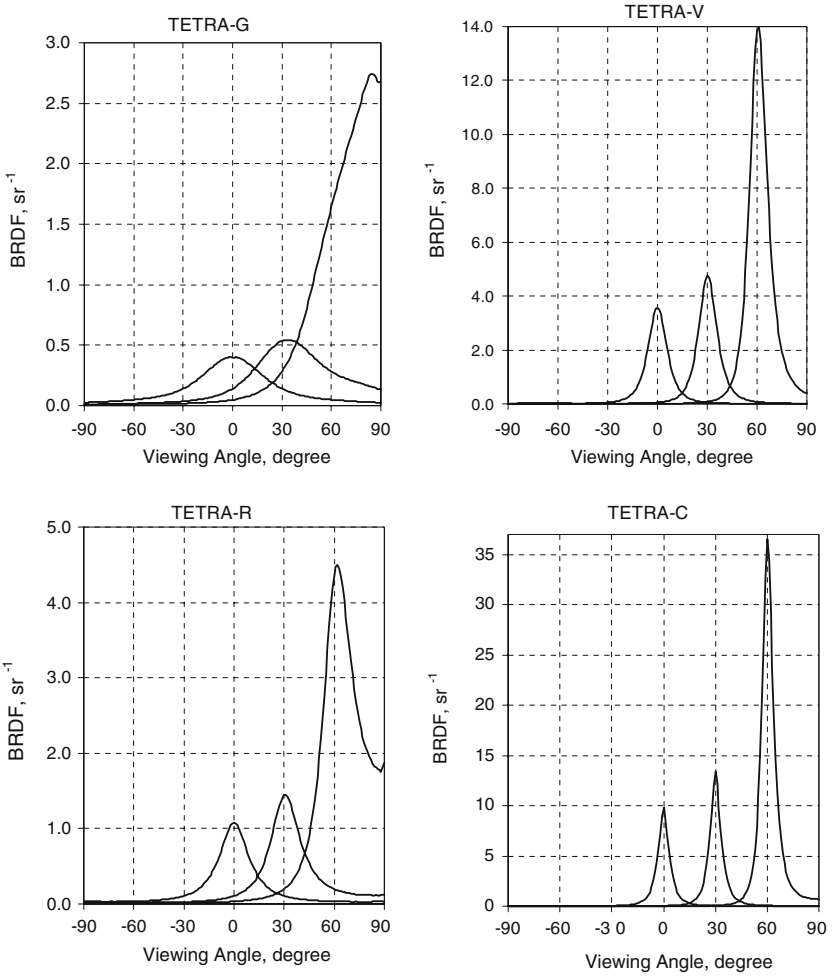

Fig. 3 In-plane TETRA-G, TETRA-V, TETRA-R, and TETRA-C BRDFs generated for $\beta = 2$, $\eta = 0.1$ and incident angles of 0°, 30°, and 60°

The models produce nearly Gaussian lobes for small η and exhibit such physical effects as off-specular peaks of reflection and enhanced backscattering for larger η. The resulting BRDFs were found to adhere to both the energy conservation law and the reciprocity principle.

2.5 Combined Models of Reflection

The combined model of reflection is the weighted sum of m components:

$$f\left(\lambda, \theta_{\mathrm{i}}, \varphi_{\mathrm{i}}, \theta_{\mathrm{r}}, \varphi_{\mathrm{r}}\right) = \sum_{i=1}^{m} A_i f_i\left(\lambda, \theta_{\mathrm{i}}, \varphi_{\mathrm{i}}, \theta_{\mathrm{r}}, \varphi_{\mathrm{r}}\right), \tag{18}$$

where A_i is the positive partial weight of i-th component, $\sum_{i=1}^{m} A_i = 1$.

This model can be fitted to experimental data by selection of A_i, the types of lower vertex projection arrangement, and by varying n_λ, k_λ, β, and η for each component.

3 Algorithm and Code Features

Currently, the following cavity shapes are implemented: axisymmetric, formed by rotation of an arbitrary polygonal section around an axis; cylindrical, with an inclined flat bottom; and a set of rectilinear grooves of polygonal profile. An arbitrary temperature distribution is determined by values in the nodes of a uniform 1D or 2D mesh. The temperature at the point of a ray-surface interaction is computed using linear or bi-linear interpolation. A number of different temperature distributions can be assigned to the same nodes to model several related tasks in a single run. The algorithm allows modeling of several conditions of observation: along an infinitely thin ray, in parallel rays, within a divergent or convergent beam, from a cavity to a circular or rectangular detector, etc., and to compute values of effective emissivity and radiance temperature.

Backward ray tracing, in which a ray originates at the detector surface and propagates toward the cavity, is applied to the computation of radiance due to contributions accrued by thermal radiation at every point of reflection. For a combined model of reflection, after every intersection of a ray with the cavity surface, the type of reflection is determined using the random numbers uniformly distributed on the interval (0, 1]. For the TETRA BRDF model, the local Cartesian coordinate system is used at the point of reflection, then the random tetrahedron is generated, and the ray traced inside the tetrahedron until it escapes. Then we return to the global coordinate system and the ray tracing continues. The trajectory formed by multiple reflections of a ray inside the cavity stops when a ray escapes the cavity or the contribution of succeeding reflections becomes negligible. The local directional spectral effective emissivity of a cavity having an arbitrary temperature distribution over a radiating surface can be computed by the following equation:

$$\varepsilon_e\left(\lambda, T, \boldsymbol{\xi}_0, \boldsymbol{\omega}_0\right) = \frac{1-\rho\left(\lambda, \boldsymbol{\xi}_0, \boldsymbol{\omega}_0\right)}{NL_{\lambda,\mathrm{bb}}\left(\lambda, T\right)} \sum_{i=1}^{N} \sum_{j=1}^{m_i} L_{\lambda,\mathrm{bb}}\left(\lambda, T_{ij}\right) \prod_{k=0}^{j-1} \rho\left(\lambda, \boldsymbol{\xi}_{ik}, \boldsymbol{\omega}_{ik}\right), \tag{19}$$

where $\boldsymbol{\omega}_{ik}$ is the direction of incidence of the i-th ray onto the k-th point of reflection $\boldsymbol{\xi}_{ik}$; $\boldsymbol{\xi}_0$ and $\boldsymbol{\omega}_0$ are the viewing point and viewing direction, respectively; ρ is the DHR (for each surface, the DHR for a set of incident angles θ_i are computed prior to ray tracing; during ray tracing, the interpolation is used); T is the reference temperature; λ is the wavelength; $L_{\lambda,\mathrm{bb}}$ is the spectral radiance of a perfect blackbody expressed by Planck's law; T_{ij} is the temperature at the point of the j-th reflection of the i-th trajectory; N is the number of rays traced, and m_i is the number of reflections in the i-th trajectory.

The random component of the computational uncertainty decreases as $N^{-1/2}$. Numerical experiments show that, in most cases, it is sufficient to use 10^7 rays to reach a random uncertainty of 2×10^{-5} or less in the effective emissivity.

4 Case Studies

4.1 Local Normal Effective Emissivities of Isothermal Conical and Cylindrical Cavities

Isothermal conical and cylindrical cavities with diffuse, specular, or specular–diffuse walls have been intensively studied in early work [25–27]. It is generally assumed that a specular conical cavity is a very "black" radiator, but a specular cylinder is a poor approximation of an ideal blackbody. In fact, a coaxial ray launched into the conical cavity with an apex angle of 30° and a wall specular reflectance of 0.1 leaves the cavity after six consecutive reflections; this ensures an effective emissivity of 0.999999. For a specular cylindrical cavity, whose flat bottom reflects all coaxial rays back outside the cavity in one reflection, the effective emissivity is 0.9. The presence of a diffuse component of reflection leads to a decrease of the effective emissivity for a conical cavity and an increase for a cylindrical one [4–6]. Their behavior in the case of specular lobes remains unexamined up to date.

We calculated the distribution of the local normal effective emissivity across the apertures of the cavities shown in Fig. 4 using the TETRA-G BRDF models depicted in Fig. 5 (3D representation in spherical coordinates) and Fig. 6 (2D in-plane sections). Prior to the effective emissivity calculation, the DHR was computed for every BRDF model for incident angles $0° \leq \theta_i \leq 90°$ with an increment of 1° (see Fig. 7, 1st family of curves). We assumed that the reflection from a tetrahedron's facets obeys the Fresnel law and that $n_\lambda = 2.5$ and $k_\lambda = 2.0$.

The results of the calculations are presented in Figs. 8 and 9. For comparison, we also performed the calculation within the framework of the conventional specular–diffuse model where the reflectance ρ was chosen to be numerically equal to the Fresnelian reflectance for normal incidence; ρ and diffusity D (the ratio of diffusely reflected radiant flux to the total one) are both independent of incident angle. Figures

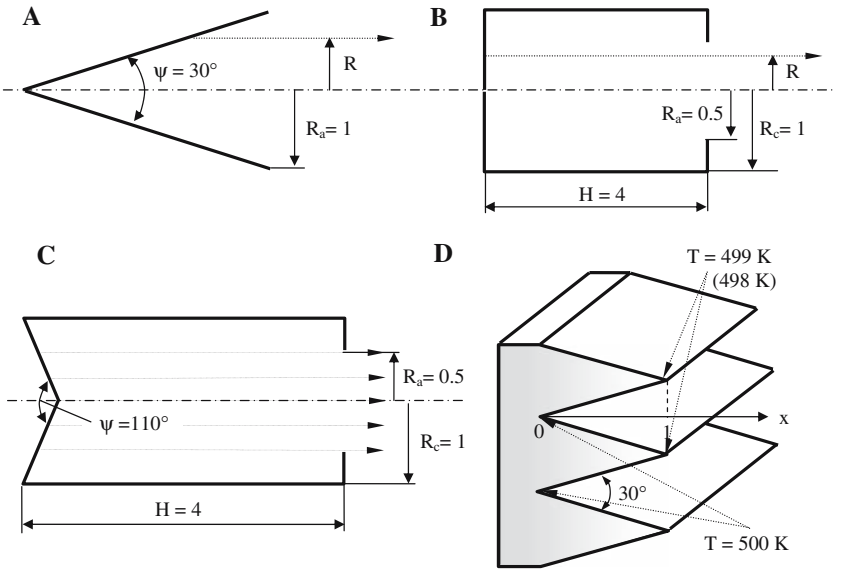

Fig. 4 Geometry of (**A**) isothermal conical, (**B**) cylindrical, and (**C**) cylinder-inner-cone cavities; (**D**) is a flat radiator with parallel V-grooves

8 and 9 exhibit significant differences in the distributions obtained for the two models. None of the dependencies computed for the TETRA model can be approximated by the dependencies computed for the specular–diffuse model with diffusity D. Calculations (Fig. 9) of the local normal effective emissivity of a cylindrical cavity using the TETRA model also predict substantively greater non-uniformity over the cavity aperture than that for the specular–diffuse model.

4.2 Isothermal Cylindro-inner-conical Cavity

We computed the dependence of the normal effective emissivity, averaged over the aperture of a cylindro-inner-conical cavity (see Fig. 4c), on the roughness parameter η; the TETRA-G BRDF model with $\beta = 2$ was used for the cavity's internal surface. The computations were also performed against diffusity D for the specular–diffuse model of reflection having the same DHR as that of the TETRA-G model at normal incidence. Both dependencies are depicted in Fig. 10. For the specular–diffuse model, the effective emissivity curve has a minimum of 0.9946 at $D \approx 0.6$. For the TETRA-G model, the effective emissivity decreases sharply for small η. This shows that the use of a purely specular model for a glossy black coating [28] can be a source of significant uncertainty. For $\eta > 0.4$, the backscattering component of reflectance appears and grows, which leads to a further decrease of the effective emissivity.

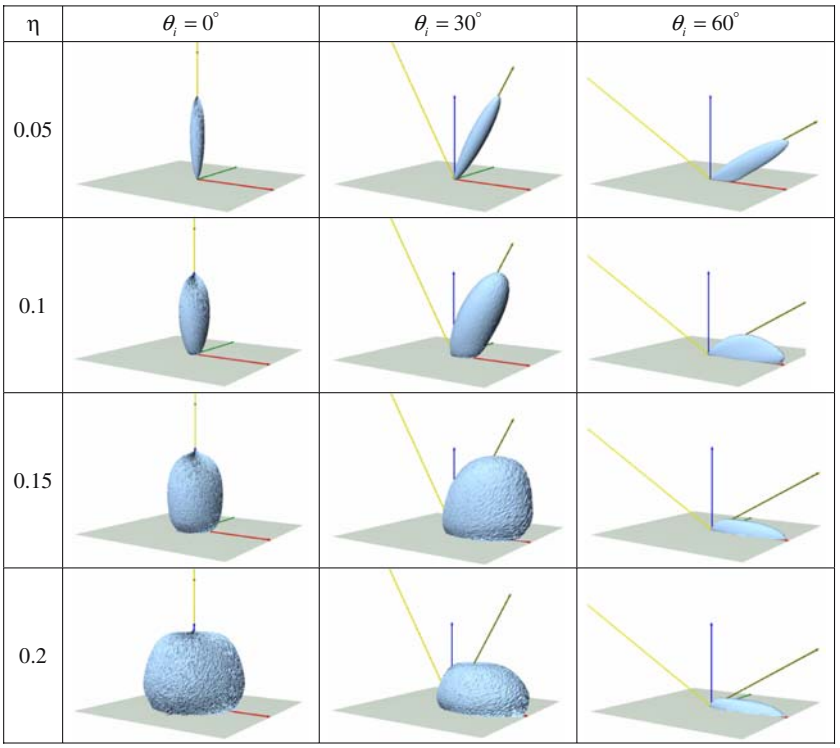

Fig. 5 3D plots of TETRA-G BRDF in spherical coordinates for three incident angles; $\beta = 2$, $n_\lambda = 2.5$, $k_\lambda = 2.0$, $\lambda = 10.6\,\mu$m. All BRDF maxima are normalized to unity

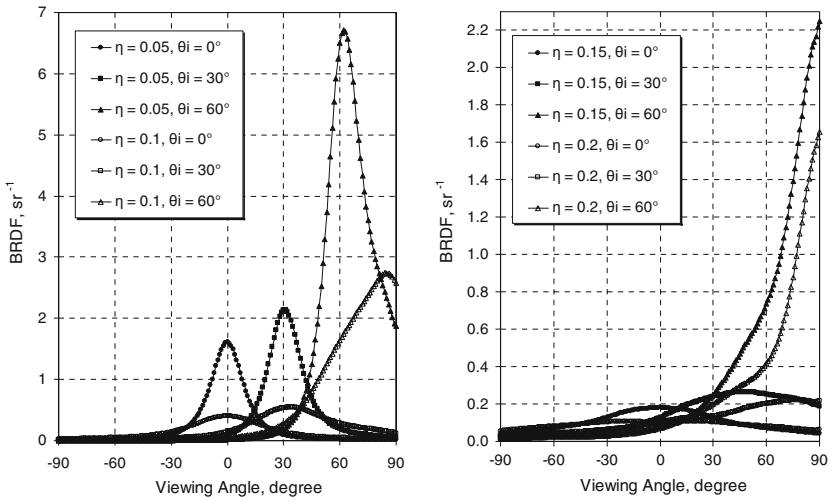

Fig. 6 In-plane TETRA-G BRDFs for various values of η and θ_i

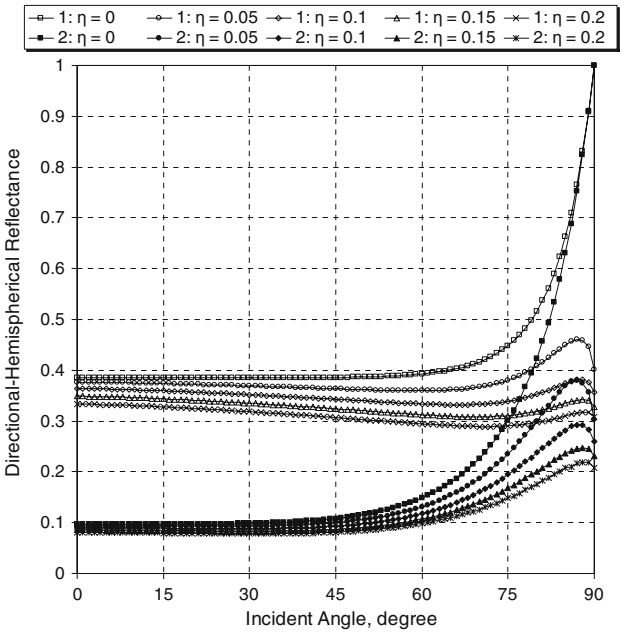

Fig. 7 DHR computed for two TETRA BRDF models with various η; 1: (for isothermal cone and cylinder modeling)—$n_\lambda = 2.5, k_\lambda = 2.0$, Fresnelian reflectance of the tetrahedron's facets; 2: (for cylinder-inner-cone and V-grooves modeling)—$\rho(0) = 0.1$, Schlick approximation for the reflectance of the tetrahedron's facets

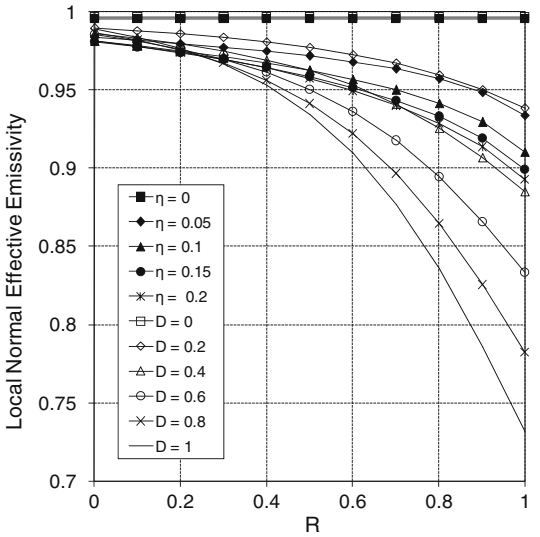

Fig. 8 Distributions of the local normal effective emissivity across the aperture of an isothermal conical cavity computed for the TETRA and specular–diffuse models of reflection

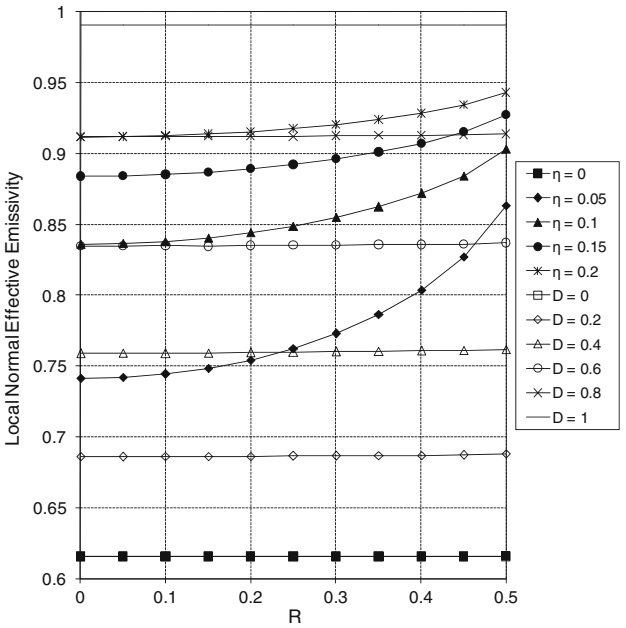

Fig. 9 Distributions of the local normal effective emissivity across the aperture of an isothermal cylindrical cavity computed for the TETRA and specular–diffuse models of reflection

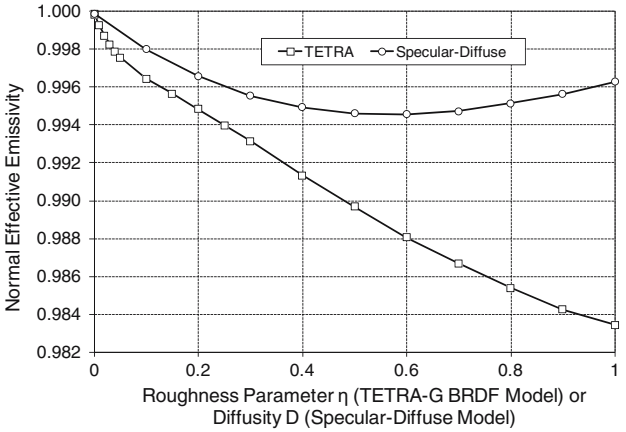

Fig. 10 Dependences of the normal effective emissivity of a cylindro-inner-cone on the roughness parameter η (TETRA BRDF model) and on diffusity D (specular–diffuse model)

4.3 Non-isothermal V-Grooved Radiator

We considered blackbody radiators in the form of a flat plate with rectilinear grooves of a triangular profile with a 30° span angle (see Fig. 4d), having a base temperature of 500 K that decreases linearly by 0, 1, and 2 K toward the groove edges. The Schlick's approximation [29] of the Fresnel sequations,

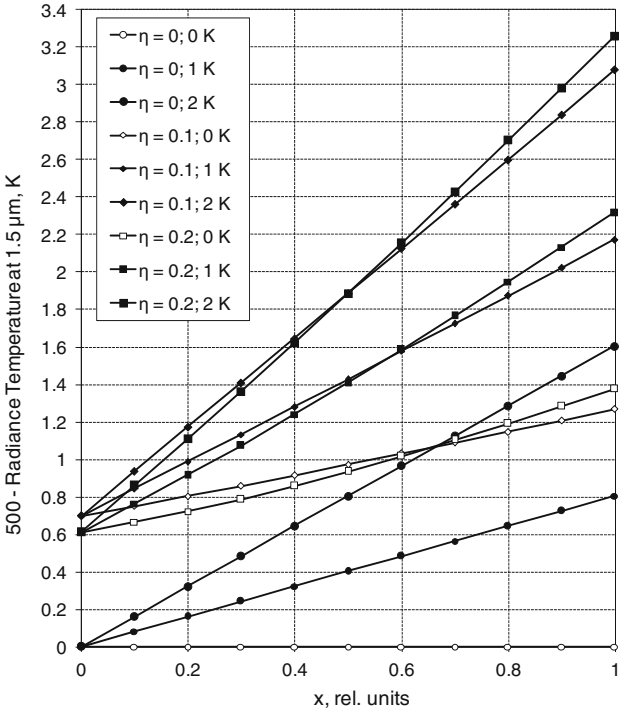

Fig. 11 Distributions of the difference between true and radiance temperature at 1.5 μm along the depth of the V-grooves for temperature drops of 0, 1, and 2 K

$$\rho\left(\lambda, \theta_{\mathrm{i}}\right) \approx \rho\left(\lambda, 0\right) + \left(1 - \cos\theta_{\mathrm{i}}\right)^{5} \left(1 - \rho\left(\lambda, 0\right)\right) \tag{20}$$

with $\rho(0) = 0.1$ was adopted for tetrahedral facets in the TETRA model of a black coating. The 2nd family of curves in Fig. 7 shows the dependence of the DHR on incident angle for various roughness parameters η. We computed the distributions of the local normal spectral effective emissivity $\varepsilon_{\mathrm{e,n}}\left(\lambda_0, x, T\right)$ at $\lambda_0 = 1.5\,\mu$m and $T = 500$ K, and then recomputed them into the radiance temperature using Eq. 2.

The results of these calculations are presented in Fig. 11. For the isothermal case, the deviation of the radiance temperature of the radiator from its thermodynamic temperature is determined only by its effective emissivity. The normal effective emissivity of a purely specular 30°-wedge is very close to unity and the radiance temperature is coincident with the thermodynamic one. The growth of η leads to a decrease of the effective emissivity and to an increase in $T - T_{\mathrm{S}}$. The temperature drop toward the groove edge leads to an additional decrease of the effective emissivity and an increase in $T - T_{\mathrm{S}}$. The joint action of these two factors (temperature drop and roughness) produces a difference $T - T_{\mathrm{S}}$ greater than the value of the actual temperature drop across the groove. Usually, the pyrometer "views" many pitches of V-grooves and their radiation should be averaged over the pyrometer's field-of-view. The result of averaging depends on the position of the center of the visible area.

5 Conclusion

We briefly described an algorithm for Monte Carlo modeling of the radiative characteristics of non-diffuse blackbody cavities. This algorithm is used to compute the effective emissivity and radiance temperature of isothermal and non-isothermal cavities for various viewing conditions. The TETRA BRDF model of reflection from random rough surfaces can be fitted with measured BRDFs and applied to solve various problems of radiative heat transfer. The numerical examples presented confirm the importance of modeling with realistic BRDFs and illustrate the broad computational capabilities of the algorithm and code that have been developed.

Acknowledgment This work was performed under the sponsorship of the U.S. Department of Commerce, National Institute of Standards and Technology.

Nomenclature

Symbols

A_i Partial weight of the i-th BRDF in the composite BRDF
c_2 1.438769×10^{-2} (m K), second constant in Planck's law
f Bi-directional reflectance distribution function (BRDF, sr^{-1})
h Depth of the tetrahedral pit (m)
k_λ Spectral coefficient of extinction
l_i Length of the i-th side of the base triangle (m)
n_λ Spectral refractive index
$\mathbf{n}$ Normal vector to the surface at the point of reflection
N Number of rays traced
p Probability density function
T Temperature (K)
T_S Radiance temperature (K)
u Random variate uniformly distributed on (0, 1]
w Random variate Weibull-distributed on $[0, \infty)$

Greek Symbols

β Shape parameter of the Weibull distribution
δ Dirac delta-function
ε Emissivity
η Scale parameter of the Weibull distribution (roughness parameter)
θ Polar angle of the spherical coordinate system (°)
λ Wavelength (μm)
ϕ Azimuthal angle of the spherical coordinate system (°)
$\boldsymbol{\xi}$ Unit vector that indicates the position
ρ Directional-hemispherical reflectance (DHR)
ψ Vertex angle of the conical or cylindro-inner-conical cavity (°)
$\boldsymbol{\omega}$ Unit vector that indicates the direction

Subscripts

bb Blackbody
e Effective
i Incidence
r Reflection

References

1. R.E. Bedford, in *Theory and Practice of Radiation Thermometry*, ed. by D.P. DeWitt, G. D. Nutter (Wiley, New York, 1988), pp. 653–772
2. A.V. Prokhorov, Metrologia **35**, 465 (1998)
3. R.C. Corlett, ASME J. Heat Transfer **88**, 376 (1966)
4. Z. Chu, J. Dai, R.E. Bedford, in *The 5th Int. Symp. on Temperature, Its Measurement and Control in Science and Industry*, vol. 6, ed. by J. F. Schooley (AIP, New York, 1992), pp. 907–912
5. A. Ono, J. Opt. Soc. Am. **70**, 547 (1980)
6. V.I. Sapritsky, A.V. Prokhorov, Appl. Opt. **34**, 5645 (1995)
7. J. Hartmann, D.R. Taubert, J. Fischer, in *Proc. TEMPMEKO '99, 7th Int. Symp. on Temperature and Thermal Measurements in Industry and Science*, ed. by J.F. Dubbeldam, M.J. de Groot (Edauw Johannissen bv, Delft, 1999), pp. 511–516
8. J.S. Toor, R. Viskanta, Int. J. Heat Mass Transfer **22**, 883 (1968)
9. P. Beckmann, A. Spizzichino, *The Scattering of Electro-magnetic Waves from Rough Surfaces* (MacMillan, New York, 1963)
10. T. Tomitani, IEEE Trans. Nuclear Sci. **43**, 1544 (1996)
11. J. Zaworski, J.R. Welty, B.J. Palmer, M.K. Drost, J. Heat Transfer **118**, 388 (1996)
12. Y.H. Zhou, Z.M. Zhang, D.P. DeWitt, B.K. Tsai, in *9th Int. Conf. Adv. Thermal Processing of Semiconductors (RTP '2001)*, pp. 179–188
13. G.J. Ward, Comput. Graphics **26**, 265 (1992)
14. A.V. Prokhorov, L.M. Hanssen, in *Proc. of SPIE*, vol. 5192, *Optical Diasgnostic Methods for Inorganic Materials III*, ed. by Leonard M. Hanssen (2003), pp. 141–157
15. F.E. Nicodemus, J.C. Richmond, J.J. Hsia, I.W. Ginsberg, T. Limperis, *NBS Monograph 160* (National Bureau of Standards, Gaithersburg, Maryland, 1977)
16. R. Srinvasan, *Importance Sampling. Applications in Communications and Detection* (Springer-Verlag, Berlin, 2002)
17. R. Siegel, J.R. Howell, *Thermal Radiation Heat Transfer*, 4th edn. (Taylor & Francis, New York, 2002)
18. K.E. Torrance, E.M. Sparrow, J. Opt. Soc. Am. **57**, 1105 (1967)
19. R.E. Walpole, R.H. Myers, S.L. Myers, Y. Keying, *Probability and Statistics for Engineers and Scientists*, 2nd edn. (Prentice Hall, Upper Saddle River, New Jersey, 2002), pp. 172–173
20. J.E. Gentle, *Random Number Generation and Monte Carlo Methods* (Springer-Verlag, New York, 1998)
21. E.W. Weisstein, "Triangle Point Picking," from *MathWorld – A Wolfram Web Resource* (2007), http://mathworld.wolfram.com/TrianglePointPicking.html
22. T. Möller, B. Trumbore, J. Graphics Tools **2**, 21 (1997)
23. B. Cabral, N. Max, R. Springmeyer, *ACM SIGGRAPH '87 Conf. Proc.*, vol. 21 (1987), pp. 273–282
24. G.V.G. Baranoski, J.G. Rokne, J. Visualization Comput. Animation (Selected papers of the Sixth Pacific Conf. on Computer Graphics and Applications – Pacific Graphics'98, Singapore, October, 1998) **10**, 225 (1999)
25. R.J. Chandos, R.E. Chandos, Appl. Opt. **13**, 2142 (1974)
26. T.J. Quinn, Infrared Phys. **21**, 123 (1981)
27. R.E. Bedford, C.K. Ma, J. Opt. Soc. Am. **64**, 339 (1974)
28. M.J. Persky, Rev. Sci. Instrum. **70**, 2193 (1999)
29. C. Schlick, Comput. Graphics Forum (Proc. Eurographics'94) **13**, 233 (1994)